

Hygroscopicity of Aerosol Particles at Low Temperatures. 1. New Low-Temperature H-TDMA Instrument: Setup and First Applications

E. WEINGARTNER,* M. GYSEL, AND U. BALTENSBERGER

Laboratory of Atmospheric Chemistry, Paul Scherrer Institut, 5232 Villigen, Switzerland

A hygroscopicity tandem differential mobility analyzer (H-TDMA) is described that allows a fast and accurate determination of the water uptake by submicrometer aerosol particles at temperatures below 0 °C. To avoid volatilization of semivolatile particles, the humidification works without heating the gas stream, and the gas-phase composition is not changed during the analysis. The applied scanning mobility analysis allows a fast and accurate measurement of the humidogram, but care has to be taken with too high scanning velocities leading to artifacts in the particle size measurement. During a field campaign at a high-alpine site (Jungfraujoch, 3580 m above sea level), humidograms of free tropospheric particles were measured at $T = -10$ °C. The hygroscopic growth of these particles was characterized by monomodal growth distributions, which means that in the observed size range (dry particle diameters (D_0) = 50–250 nm) the free tropospheric aerosol was to a large extent internally mixed. No distinct deliquescence was observed, indicating that the multi-component aerosol particles are present in a liquid state even at a low relative humidity (RH) < 10%. At RH 85%, average hygroscopic growth factors of 1.44, 1.49, and 1.53 were measured for $D_0 = 50, 100,$ and 250 nm. The estimated soluble volume fraction of the particles in the observed size range was found to be 0.79, 0.86, and 0.91, respectively.

Introduction

The hygroscopic properties of the atmospheric aerosol play a crucial role in air quality, acid deposition, biochemical cycles, visibility reduction, and formation of clouds and precipitation. In recent years, the impact of aerosol particles on climate change has been recognized. While the combined positive climate forcing of the greenhouse gases can be fairly well estimated, the complexity of the aerosol–cloud–climate system makes the negative forcing due to atmospheric aerosols the largest current source of uncertainty in predictions of the future global climate (1). The atmospheric aerosol affects the earth's radiation balance in two ways, directly and indirectly. Aerosol particles influence the climate directly by absorbing as well as reflecting the incoming short-wave solar radiation back to space. This capability is strongly dependent on the particle size, which is itself a function of

the relative humidity (RH). It is well-known that, in the presence of water vapor, the size of an aerosol particle may increase by 1.1–2.5 times as compared to its original “dry” size over the RH range of 30–95%, depending on aerosol composition (2–4). The number size distribution and the hygroscopic properties of the aerosol also determine which fraction of aerosol particles can act as cloud condensation nuclei (CCN) and thus contribute to the indirect aerosol effect. This effect refers to the fact that an increased number of cloud droplets may alter the microphysical properties of clouds (5).

The response of aerosol particles to changes in RH can be measured with a variety of instruments. The water content as a function of RH may be obtained either by weighing a bulk aerosol sample (6), by an elemental analyzer (7), by the Karl Fischer method (8), or by determining the growth factor of aerosol particles under enhanced RH conditions. The latter is possible by means of the single-particle levitation technique (9–11) or a hygroscopicity tandem differential mobility analyzer (H-TDMA) (12, 13).

In the field, hygroscopicity measurements are commonly performed using humidity-controlled nephelometry (14) or by means of a H-TDMA. The latter technique has been used at a number of sites around the globe (15–24). Most of these measurements have been performed in the planetary boundary layer, and it was often found that the submicrometer aerosol particles were characterized by two or more modes of hygroscopic growth rather than a broad distribution of growth. This means that, near sources, the aerosol is in many cases externally mixed regarding its hygroscopic properties.

All of these measurements have been performed at room temperature (20–30 °C), which may differ from ambient temperature. However, the gas temperature may significantly influence the partitioning of components between the particulate and the gas phases and thus change the hygroscopic behavior of particles. The organic fraction of particulate matter in both rural and urban areas is a complex mixture of many compounds. Recent studies have shown that organic material may considerably alter the hygroscopic properties of aerosol particles (25). Saxena et al. (26) used H-TDMA and impactor data from the Grand Canyon and Los Angeles in the United States and concluded that organic material from freshly produced aerosol particles hindered hygroscopic growth, while organic species in particles found in aged air masses seemed to increase growth. Semivolatile inorganic compounds are also important. Ammonium nitrate losses during sampling have been reported in numerous studies. Russell et al. (27) estimated that at temperatures greater than 30 °C most nitrate will be in the gas phase as nitric acid (HNO_3), while at temperatures lower than 15 °C most nitrate is present in the particulate phase. The relative humidity and the concentration of ammonia and nitric acid gases also affect the equilibrium, but temperature is by far the most important variable.

The aerosol indirect effect occurs also in the middle and upper troposphere, i.e., in the -40 °C < T < 0 °C temperature range. If under these conditions the aerosol is heated to room temperature, nitrate or semivolatile organics may desorb from particles and considerably alter their hygroscopic properties. Therefore, at these altitudes, hygroscopic properties of aerosol particles have to be measured at ambient temperatures to prevent artifacts due to volatilization of semivolatile compounds. An ideal location to perform such studies is the high-alpine site Jungfraujoch (JFJ) at 3580 m above sea level (46.55° N, 7.98° E). It is situated on the northern side of the main central European alpine

* Corresponding author e-mail: ernest.weingartner@psi.ch; phone: 0041 56 310 24 05; fax: 0041 56 310 45 25.

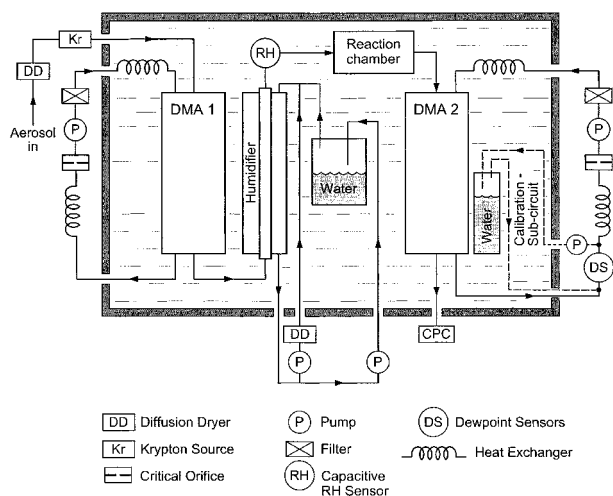


FIGURE 1. Sketch of the low-temperature H-TDMA. The main components are submersed in a water/ethylene glycol bath ensuring constant temperature.

chain in Switzerland with ambient average temperatures of $-1\text{ }^{\circ}\text{C}$ in summer and $-14\text{ }^{\circ}\text{C}$ in winter and is perennially covered by snow. Since July 1995, the JFJ station has been conducting measurements under the Global Atmosphere Watch (GAW) program of the World Meteorological Organization (WMO). During the summer, JFJ is often influenced by the planetary boundary layer (PBL) through thermally driven aerosol transport in the afternoon, while at other times and seasons the site is mainly located in the free troposphere (FT) (28). Several studies on atmospheric aerosols have been previously conducted here (29–34), with most aerosol measurements being performed indoors at $20\text{--}30\text{ }^{\circ}\text{C}$.

In this work a new version of a H-TDMA is introduced that is capable of measuring the hygroscopic growth of aerosol particles at temperatures below $0\text{ }^{\circ}\text{C}$. The operating principle of the low-temperature H-TDMA is presented, and the advantages and limitations of the scanning mobility analysis are investigated. A measurement of the humidogram of $(\text{NH}_4)_2\text{SO}_4$ particles at $20\text{ }^{\circ}\text{C}$ is then discussed, and field measurements at the high-alpine site JFJ are presented. The hygroscopicity of aerosol particles in the free troposphere was measured at this site at ambient temperatures ($T = -10\text{ }^{\circ}\text{C}$) with high temporal resolution. In the second part of this work (35), a detailed discussion of the hygroscopic properties of laboratory-generated $(\text{NH}_4)_2\text{SO}_4$, NaCl, and NaNO_3 particles at 20 and $-10\text{ }^{\circ}\text{C}$ and the agreement with theory is discussed.

Experimental Section

This instrument was designed to meet the following demands: (i) The hygroscopicity of particles with diameters between 20 and 250 nm can be determined in the temperature and RH ranges $-20\text{ }^{\circ}\text{C} < T < 30\text{ }^{\circ}\text{C}$ and $10\% < \text{RH} < 90\%$ with an accuracy of $0.1\text{ }^{\circ}\text{C}$ and $<1.6\%$, respectively. (ii) The acquisition time of one size scan is $<5\text{ min}$. (iii) For a sufficiently high aerosol concentration, the change in particle mobility diameter is measured with an accuracy of $<1\%$. (iv) The gas-phase composition is not changed during the measurement, and the humidifier works without changing the gas temperature. (v) The instrument is robust, suited for field experiments, and measurements can be conducted in stand-alone operation.

General Working Principle. Figure 1 shows the experimental setup of the low-temperature H-TDMA. All components and tubing that need to be held at constant temperature are located inside an isolated cylinder (stainless steel, volume = 20 L) and are submersed in a water/ethylene glycol bath.

This bath is connected in a closed loop arrangement to a cooling/heating unit. The liquid is recycled once per minute, which ensures a temperature gradient $\Delta T < 0.1\text{ }^{\circ}\text{C}$ at $T = -10\text{ }^{\circ}\text{C}$ inside the cylinder. The bath temperature determines the temperature at which the hygroscopic properties are measured.

First, the aerosol (flow rate: 0.3 L min^{-1}) enters a silica gel diffusion dryer designed for operation at low temperatures ($T = -20\text{ }^{\circ}\text{C}$) to dry the sample to a frost point temperature of $T_f < -30\text{ }^{\circ}\text{C}$. This corresponds to a $\text{RH} < 15\%$ for $T > -10\text{ }^{\circ}\text{C}$. If a lower RH is required, the aerosol can additionally be dried with a phosphorus pentoxide dryer. The dry aerosol is then charged with a diffusion charger (^{85}Kr) and fed into the main part of the H-TDMA where the measurement involves three steps. In a first differential mobility analyzer (DMA1), a narrow size range of the dry aerosol is selected. This monodisperse aerosol is conditioned to a well-defined higher RH and fed into a chamber with a residence time of 1 min . Although water vapor equilibration times are very short for pure submicrometer particles (milliseconds or shorter), the high residence time was chosen because it is known that organic films may impede the transfer of water across the particle surface and thus increase the characteristic time scale for water vapor to reach equilibrium with the particles (26). The aerosol particle diameter at this new RH is then measured using a second DMA (DMA2) and a condensation particle counter (CPC). The DMAs are TSI 3071 types, where the HV connector was modified to allow submersed operation. To avoid any heat bridges, the DMAs and all other critical parts have no thermally conducting contact to the cylinder walls. In the H-TDMA presented in this paper, a TSI 3022A CPC was used to count particles. However, using a different CPC (such as a TSI 3010 or 3760) would be an improvement to our system, since these CPCs have a higher flow rate leading to better counting statistics and to a smaller response time (see below). For the determination of hygroscopic growth factors (D/D_0), defined as the ratio of the humidified particles diameter (D) to the dry particle diameter (D_0), a precise measurement of D as well as D_0 is required. Although D_0 can be calculated, in practice, D_0 is periodically measured simply by “switching off” the humidifier and thus lowering the RH in DMA2 to the low RH present in DMA1. The value of D_0 determined in this manner is used as the reference dry diameter for further calculations. This procedure increases the quality of the data because the low RH in DMA1 is checked and instrumental drifts in the diameter measurements are easily identified.

Sheath Airflow System. The H-TDMA was designed to maintain the gas-phase composition by using recirculating air streams; however, one has to consider that the chemical composition of particles may have changed during the drying process in the diffusion drier. For example, NH_4NO_3 particles will to some extent volatilize in the diffusion drier when they are transferred from a humid to a dry environment. The reverse may occur in the humidifier when, for example, a sample with high HNO_3 gas-phase concentration is exposed to high RH leading to a transfer of nitric acid to the aerosol phase. Apart from the stability of the flows, operating the DMAs in a closed-loop arrangement also has the advantage of being relatively simple and robust. Great care has to be taken that the pumps are absolutely airtight. This is of great importance because a leak of, for example, 1% would cause a change in the aerosol flow of about 10% . Another critical point is that the pump works at a temperature of approximately $50\text{ }^{\circ}\text{C}$. Outgassing material from inside the pump (e.g., from rubber membranes or O-rings) may condense at lower temperature inside the H-TDMA and significantly change the aerosol and gas-phase composition. For the instrument presented in this paper, airtight pumps were used operating with Teflon membranes, thus avoiding any artifact

by outgassing material. The sheath airflows (3.5 L min^{-1}) are controlled by critical orifices located in the excess air outlet of the DMAs. The critical operation of the orifices is guaranteed by monitoring the vacuum pressure with pressure sensors. The pulsation in the air exiting the pump is removed with a valve, which generates a slight overpressure of 200 mbar inside the pump.

After particle filtration, the sheath air is fed to a heat exchanger located inside the water/ethylene glycol bath. This exchanger was designed such that air with $T = 30 \text{ }^\circ\text{C}$ is assimilated with $\Delta T < 0.1 \text{ }^\circ\text{C}$ to a bath temperature of $-10 \text{ }^\circ\text{C}$. Care was taken in designing the exchanger of the second DMA such that no moisture is lost by condensation caused by the pressure increase in the heat exchanger.

RH Generation, Measurement, and Calibration. The dry and monodisperse aerosol exiting DMA1 is humidified by passing it through a vertically oriented Gore-Tex tube (0.6 cm i.d., 40 cm long). This tube is located inside another tube where a secondary air stream is circulating in counter flow direction (flow rate: approximately 3 L min^{-1}). Moisture can diffuse from this secondary flow through the Gore-Tex membrane into the aerosol stream. The secondary airflow circulates in a closed-loop arrangement and is branched up into a saturated and dry path. The RH is determined by the airflow ratio through these branches. This is realized with a PID controller that controls the pump power in both branches by comparing a set RH with that measured by a capacitive sensor (HP101A, Rotronic). To prevent an overshoot in RH, the saturator of the humidified branch is also located inside the water/ethylene glycol bath. This humidifier works without heating the aerosol and is able to generate RHs up to 90% even at temperatures below $0 \text{ }^\circ\text{C}$.

The RH inside DMA2, which finally determines the measured particle size, is deduced from precise measurement of the bath and dew point temperature. The temperature is measured at the upper and lower part of the bath (i.e., at the entrance and exit of the DMA) by means of PT100 resistors. The dew point is monitored in the excess air of the DMA with two dew point sensors (model 2002 Dewprime, EdgeTech, and model 911 Dew-all, EG&G). Since the dew point temperature measurement depends on air pressure, care was taken to avoid a significant pressure drop between DMA2 and the sensors. The utilization of two dew point sensors increases the reliability, as malfunctioning of one instrument (such as contamination of the mirror surface) is easily detected by comparison.

The measured dew points are periodically checked with a separate calibration loop, where filtered air is saturated with water vapor at a certain bath temperature and fed into the dew point sensors. A heat exchanger before the saturator ensures that at low temperatures the air is saturated at the bath temperature. This allows an internal calibration of the dew point sensors by adjusting the measured dew point temperatures to the bath temperature measurements in the data acquisition program. With this procedure the bath and dew point temperature measurement is achieved with an accuracy of $0.15 \text{ }^\circ\text{C}$ for each value, which transforms to a RH accuracy of 1.1% at 90% for $T = 20 \text{ }^\circ\text{C}$ and 1.6% at 90% for $T = -10 \text{ }^\circ\text{C}$.

Measurement at $T < 0 \text{ }^\circ\text{C}$. The selected particle mobility diameter in the DMA is a function of gas temperature and pressure. The data analysis takes into account that the volumetric flows, the air viscosity, and the gas mean free path are temperature and pressure dependent.

For $T < 0 \text{ }^\circ\text{C}$, frost points are measured by the dew point sensors. These temperatures are converted in the data evaluation into dew points, and RH is always calculated with respect to liquid water unless otherwise mentioned.

Principally, $T < 0 \text{ }^\circ\text{C}$ measurements are conducted in a manner similar to those at $T = 20 \text{ }^\circ\text{C}$. The water in the

humidifier and RH calibration circuit will freeze and fulfill their service by saturating the air with respect to ice. Experimental difficulties may arise if the secondary airflows of the humidifier freeze up, leading to a plugging of the airstreams. Such a freezing of the tubing occurs when the H-TDMA is cooled off to a lower working temperature and high RH is already present in the system. In such a case, one has to defrost and dry the whole system. At JFJ, the instrument was continuously operated during 4 weeks at $T = -10 \text{ }^\circ\text{C}$ and the hygroscopic growth was predominately measured at RH 85%. A drop in performance of the humidifier was temporarily observed after 1 week of continuous operation at this high RH. We assign this to a plugging of pores with ice in the Gore-Tex material, reducing the permeability of the tube. In this situation, a simple reduction of the humidifier RH set point during a period of approximately 4 h often solved this problem—a procedure that was also used to check the reference dry diameter (D_0).

In this and the companion paper (35), we will present measurements performed at $T < 0 \text{ }^\circ\text{C}$ in the field as well as in the laboratory. For all laboratory experiments, particles were generated, dried, charge-neutralized at room temperature ($T = 20 \text{ }^\circ\text{C}$), and cooled for the first time inside the H-TDMA. For the field measurement at JFJ, great care was taken to maintain the original aerosol composition. The sampling head, diffusion dryer, charger, and all tubing were kept at ambient temperature. The continuously monitored RH of the aerosol entering the H-TDMA was always $< 10\%$.

Process Control and Data Processing. Stand-alone operation is made possible by using a custom-written LabView program running on a personal computer. Analog-to-digital and digital-to-analog converters are used to monitor temperature and RH measurements as well as to change the applied DMA voltages and RH set points. The aerosol size spectra of humidified particles may be obtained by changing the voltage on DMA2 either in discrete steps or continuously. In the first method, also called differential mobility particles sizer (DMPS), a fixed voltage is applied, and after a certain waiting time, the particle number concentration exiting the DMA is measured. This method is often applied in H-TDMA analysis because it ensures high accuracy of the diameter measurement. The main disadvantage of this method is a low time resolution, which may cause problems with the measurement of rapidly changing particle size distributions (the overall scan time, a function of the number of size bins, is typically 15 min). In the second method, also called scanning mobility particle sizer (SMPS) (36, 37), the applied voltage at the DMA center rod is continuously increased in magnitude, and the CPC signal is monitored with a sampling rate of 0.1 Hz. With this method, a scan with a high size resolution can be achieved within 60 s or less. At low number concentrations subsequent scans can be averaged to improve particle counting statistics. For both measuring methods, LabView subroutines were written and embedded in the main program. This allows different dry particle sizes to be measured and an optimal automatic adjustment of the scanned diameter ranges.

Results and Discussion

Comparison of Stepping and Scanning Mobility Analysis (DMPS vs SMPS). First, the application of the SMPS routine in the present instrument will be discussed. We will show that care has to be taken with too short scan times resulting in high scanning velocities (v_s). Since the applied voltage is increased exponentially with scanning time in most applications, we define v_s as the change in diameter on a logarithmic scale per time:

$$v_s = \frac{d \log D}{dt} \quad (1)$$

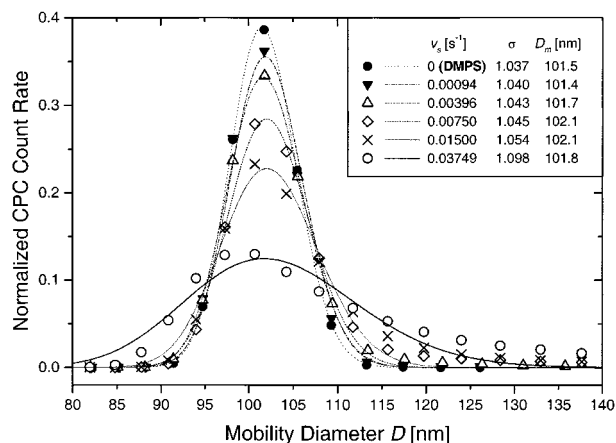


FIGURE 2. Comparison of H-TDMA spectra measured under dry conditions with the DMPS and SMPS methods for different scanning velocities (v_s). The standard deviation (σ) and the modal diameter (D_m) of the spectra are deduced by fitting the measured data (symbols) with log-normal size distributions (lines, eq 2). The SMPS measurement was corrected with a “true” delay time of $t_d = 3.4$ s resulting in modal diameters that are fairly independent of the scanning velocity. For $v_s > 0.004$ s $^{-1}$, the impairment of the resolution appears in higher σ values.

This definition results in nearly constant values of v_s over the scanned diameter range.

Figure 2 shows H-TDMA size spectra measured with the SMPS technique for different scanning velocities as well as a DMPS spectrum for comparison. $(\text{NH}_4)_2\text{SO}_4$ particles were produced by atomization of an aqueous solution and subsequent diffusion drying. The spectra were measured with DMA2, while the first DMA was operating at a fixed voltage selecting particles with $D_o = 101.5$ nm. To investigate the influence of the scanning velocity on the shape of the size spectra, the particles were not humidified ($\text{RH} < 10\%$ in the humidifier), and the measurement was performed at $T = 20$ °C. The size spectra were fitted with log-normal size distributions:

$$\frac{dN_c}{d \log D} = \text{constant} \exp\left(-\frac{(\log(D) - \log(D_m))^2}{2 \log^2(\sigma)}\right) \quad (2)$$

where N_c is the count rate (in s $^{-1}$) of the CPC, D_m is the fitted modal diameter, and σ is the standard deviation.

A high agreement between DMPS and SMPS was found for low-scanning velocities; however, for $v_s > 0.004$ s $^{-1}$, the accuracy of the particle size measurement decreased significantly. The impairment of the resolution appeared in higher σ values and in larger count rates at larger diameters. These artifacts are mainly due to a smearing effect caused by the response time of the CPC and also depend on the flow rates as well as on the type of CPC (38). One can easily imagine that a fraction of particles is buffered before and inside the CPC, resulting in a retarded detection. For our H-TDMA configuration, the smearing effect is negligible since size spectra are generally taken in small diameter size ranges resulting in $v_s < 0.002$ s $^{-1}$. However, if the SMPS technique is applied for the rapid determination of the size distribution in a larger range, the smearing effect may become important (see below).

Besides this smearing effect, high-scanning velocities may also lead to another uncertainty: The absolute diameter measurement depends strongly on the delay time (t_d), which is the average time the aerosol takes to travel from the sample extraction slot of the DMA to the point of detection in the CPC. This delay is taken into account by the SMPS software (by assuming plug flow), but an under- or overestimation of

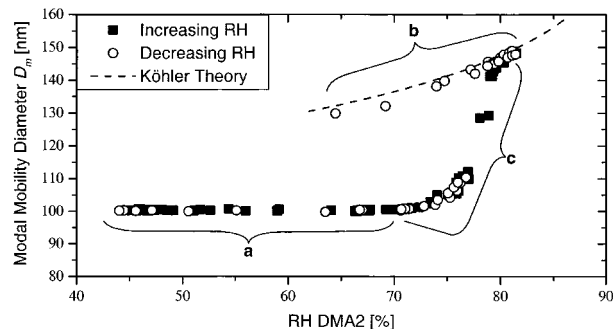


FIGURE 3. Example of a humidogram of laboratory-generated $D_o = 100$ nm $(\text{NH}_4)_2\text{SO}_4$ particles at $T = 20$ °C. Points are labeled according to increasing and decreasing RH conditions and different states of hygroscopic growth. The dotted line is a theoretical curve (see text).

t_d will shift the measured size distribution either to larger or smaller diameters. The true diameters D_{true} are related to the measured diameters D_{meas} by

$$D_{\text{true}} = D_{\text{meas}} 10^{(v_s \Delta t_d)} \quad (3)$$

where Δt_d is the error in the delay time t_d .

To determine the true t_d , the monodisperse size distributions in Figure 2 were measured assuming a certain constant t_d and were shifted laterally (by varying Δt_d) so that the average modal diameter agreed with the modal diameter measured in the stepping mode. The best agreement was found for $t_d = 3.4$ s.

The relative error in the measured diameters is given by

$$\frac{\Delta D}{D} = 10^{(v_s \Delta t_d)} - 1 \quad (4)$$

Again, this shift increases significantly for high v_s . The correct determination of t_d is of great importance if spectra are taken over a broad size range and with short scan times. For example, if spectra are taken in the diameter range of 16–630 nm with a scan time of 60 s (= default scan time of the commercially available SMPS software) the measurement will be performed with $v_s = 0.0266$ s $^{-1}$ and an error in t_d of $\Delta t_d = 1$ s will translate into a relative error of $\Delta D/D = 6.3\%$. A calculation of higher moments (such as the volume size distribution) will result in a significant enlargement of this error.

The delay time error has a negligible effect on the H-TDMA results as long as relative size changes are deduced from the spectra, such as growth factors (D/D_o). This is due to the fact that, as long as the spectra are acquired with constant v_s , the measured diameters D_{meas} are proportional to the true diameters D_{true} (see eq 3).

Measurement of Hysteresis Behavior of Particle Growth.

Humidograms of various laboratory-generated aerosols at +20 and –10 °C as well as a comparison with theoretical calculations are presented in the following and are also discussed in our companion paper (35). First, we will illustrate in detail how the RH-dependent growth of an aerosol is measured with the H-TDMA. Figure 3 shows a typical measurement of the humidogram of laboratory generated $(\text{NH}_4)_2\text{SO}_4$ particles. In this example, the H-TDMA operating temperature was set to 20 °C. The aerosol was again produced by atomization and subsequent drying of an aqueous solution, and DMA1 was operated at a fixed voltage to select $D_o = 100$ nm particles. The hygroscopic growth of the particles is characterized by a strong increase in diameter at its deliquescence humidity $\text{DRH} = 80\%$, which is due to the phase transition of particles changing from dry crystals to saturated solution droplets. We define DRH as the RH in the

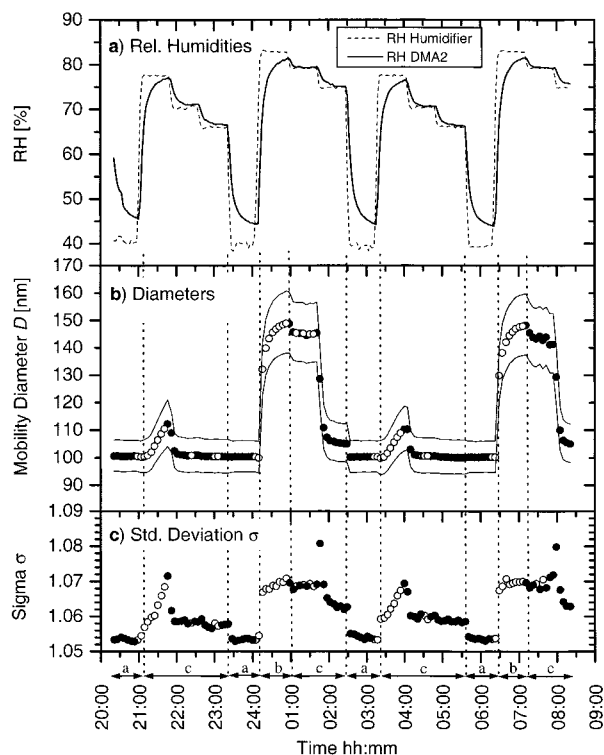


FIGURE 4. Temporal evolution of the humidogram measurements presented in Figure 3: (a) RH before and inside DMA2, (b) fitted modal diameters (points) and diameters of half-maximum (lines) giving an impression of the shape of the number size distribution, and (c) standard deviation of the size spectra. Points are labeled according to decreasing (open symbols) and increasing (closed symbols) RH conditions. Vertical dotted lines delimit conditions leading to a different hygroscopic growth (see text).

transition regime where the growth of the droplets reaches the growth of solution droplets. In this example, the phase transition is not a sharp function of RH. A distinct increase in particle size is already seen at $RH < DRH$ and will be discussed in more detail below. Due to the hysteresis phenomenon, the particles that experienced $RH > DRH$ may stay in a metastable state well below the deliquescence point, and their equilibrium size is described by the Köhler theory (39). The dashed line in Figure 3 is such a model which uses a semiempirical calculation of the water activity of $(NH_4)_2SO_4$ solutions (see Part II for more details).

Figure 4 exemplifies how this measurement was performed and how the different cases (increasing or decreasing RH scans) were determined. Figure 4a shows the temporal evolution of the RH measured just after the humidifier as well as the RH in DMA2. Since DMA2 is operated in a closed-loop arrangement, the RH inside this instrument shows a delayed response to a change of the humidifier RH set point. This circumstance is utilized to assess the development of the RH. When passing through the instrument, the aerosol experiences increasing RH when the humidifier RH set points are subsequently lowered, resulting in lower RH in the humidifier compared to DMA2. On the other hand, the aerosol experiences decreasing RH when the humidifier RH is suddenly increased, resulting in a higher RH in the humidifier.

Figure 4b shows the temporal evolution of the size distribution measured continuously by DMA2 using the SMPS technique (time resolution: 5 min; scanning velocity: $v_s = 0.0014 \text{ s}^{-1}$), which enabled 136 size spectra to be measured within 12 h. A monomodal shape was found for all measured size distributions, and the modal diameters, calculated by fitting the spectra with log-normal size distributions (eq 2),

as well as the diameters of half-maximum are also indicated. The standard deviation (σ) of the fitted spectra is shown in Figure 4c and depends on the measured modal diameters. It ranges from 1.053 to 1.060 for “dry” $D = 100 \text{ nm}$ particles and increases up to $\sigma = 1.070$ for $D = 150 \text{ nm}$ particles. A theoretical calculation has shown that the observed change in σ can be explained by $\sim 85\%$ in magnitude with the size dependent width of the DMA2 transfer function. The remaining 15% are partially attributed to morphological inhomogeneities within the monodisperse particle population.

Different symbols for the fitted modal diameter and for the standard deviations are used in Figures 3 and 4 to distinguish between conditions of increasing and decreasing RH. The determined modal diameters together with the RH in DMA2 were used for plotting the corresponding humidogram (Figure 3).

For pure NaCl and $(NH_4)_2SO_4$ particles, it was observed in many experiments that the phase transition at the deliquescence point is not a sharp function of RH. For these salts, it was found that the humidograms can be divided into three different states. In the following, this classification is exemplified on the basis of the $(NH_4)_2SO_4$ measurement, and the different states are indicated in Figures 3 and 4.

State a. The particles in the H-TDMA are always exposed to $RH < DRH$, and the RH in DMA2 (which determines the final particle size) is $< 70\%$. This results in no hygroscopic growth, and the points are located on the lower (“dry”) hysteresis branch. In this range, a reduction of the mobility diameter is often observed and is interpreted as a restructuring of the particles. For the comparison of H-TDMA measurements with theoretical growth curves, the determination of the minimal diameter D_{min} in this RH range is of great importance because D_{min} relates more closely to the volume equivalent diameter of the dry particle (see Part 2 for more details).

State b. The aerosol experienced $RH > DRH$ (either in the humidifier or in DMA2), and the RH in DMA2 is larger than the crystallization RH, which is 37% for pure $(NH_4)_2SO_4$ particles (40). For this condition the points are located on the upper (wet) part of the hysteresis branch.

State c. The particles never experienced $RH > DRH$ but the RH in DMA2 is $> \sim 70\%$. There, as already mentioned, an increase of the particle size is observed for the lower hysteresis curve. This hygroscopic behavior was observed during several measurements although often a smaller gradual onset of deliquescence at $RH < DRH$ was measured (see $(NH_4)_2SO_4$ measurements in companion paper; 35). Up to $RH \sim 77\%$, this phenomenon is observed for decreasing or increasing RH, which is a strong indication that up to this value the growth is a reversible process and that the particles are present in the form of an internally mixed phase (liquid/solid). Note that near the DRH, at RH 78–79%, two points were measured that are characterized with a relatively broad growth distribution ($\sigma = 1.08$, see Figure 4). Such a gradual onset of deliquescence was also observed in other laboratory studies for pure salt particles with a H-TDMA (41) and with light scattering techniques (14). Neubauer et al. (42) used online laser desorption ionization spectrometry to access humidity effects on single aerosol particles and observed that at $RH < DRH$ similar spectra to those of aqueous droplets were measured. They attributed this water uptake to defects such as cracks on the particles surface. Braun and Krieger (43) used an electrodynamic balance and observed a “stable” mass increase at $RH < DRH$ for micrometer sized pure NaCl particles. From the analysis of the particle light-scattering intensity fluctuation, they concluded that during deliquescence, water is taken up from the gas phase and forms an aqueous solution shell around the solid particle (44).

Field Measurements. The Cloud and Aerosol Characterization Experiment (CLACE) was organized at the JFJ

research station in Switzerland from February 2 to March 31, 2000 with the participation of eight Swiss, German, and Hungarian institutes. Besides the extensive measurement of aerosol number size distributions, optical properties, volatility, and chemical composition, the hygroscopicity of the particles was measured with two H-TDMA instruments. Our H-TDMA was operated at $T = -10\text{ }^\circ\text{C}$ while the other H-TDMA (45) measured the hygroscopic properties at room temperature ($25\text{--}30\text{ }^\circ\text{C}$). A comparison of both H-TDMA data sets combined with the data on aerosol volatility and chemical composition will yield detailed information about the nature of the particles and will be the subject of a future manuscript.

During the campaign, the hygroscopic growth of particles with $D_o = 50, 100,$ and 250 nm was continuously measured at a constant RH of 85% and at $T = -10\text{ }^\circ\text{C}$. Most of the time, the station was located in the FT, and the shape of the humidified H-TDMA size spectra were preferentially characterized by a narrow monomodal growth distribution ($\sigma < 1.08$). This implies that the particles in the observed size range were to a large extent internally mixed regarding their hygroscopic properties and hence also chemically. This is in contrast to the behavior of continental polluted aerosols where the particles generally separate into a less and more hygroscopic group. Only during temporally limited periods where the station was influenced by local pollution (mainly due to construction work), bimodal distributions with a more and a less hygroscopic mode were found. The latter mode is clearly attributed to freshly emitted combustion particles emitted from heavy-duty diesel engines, which are known to have a hydrophobic behavior (46). During periods when the station was exposed to a dust plume from North Africa, $D_o = 250\text{ nm}$ particles often exhibited bimodal growth distributions. It was found that Saharan dust particles, which were to some extent also present in the submicrometer size range, were characterized by a low hygroscopicity.

During several episodes, the RH was lowered to measure the RH dependence of the growth factors at $T = -10\text{ }^\circ\text{C}$. In this paper we will focus on two such events where the station was clearly located in the FT. Figure 5 shows humidograms measured on March 6 and 16, 2000. The data were acquired with a scanning velocity $v_s < 0.0016\text{ s}^{-1}$ and with a time resolution of 5 min. After 3 scans (i.e., after 15 min) the applied DMA1 voltage was changed such that $D_o = 50, 100,$ and 250 nm particles were measured alternately with a high temporal resolution. The acquisition of all points in Figure 5 with $20\% < \text{RH} < 80\%$ lasted only twice for 3 h. Therefore, these humidograms can be considered as a snapshot of current atmospheric conditions.

The relatively high scatter of the $D_o = 250\text{ nm}$ data is due to very low inlet concentrations: The average number size distribution over the time periods presented in Figure 5 shows concentrations of $dN/d\log D = 92, 136,$ and 63 cm^{-3} for $D_o = 50, 100,$ and 250 nm , respectively. These measurements clearly show that with the applied SMPS technique data with a good quality and a high temporal resolution can be achieved even at very low number concentrations.

It is interesting to note that the humidograms are characterized by a continuous increase of D/D_o as function of RH—no distinct deliquescence behavior is observed during these increasing RH scans. It is well-known that multicomponent aerosols may exhibit a hysteresis behavior different from pure salts, i.e., the deliquescence humidity DRH of mixed salts is always lower than the DRH of the individual salts in the particle (9). DRH is also considerably lowered by the presence of nitrate—a major ionic component found in JFJ samples. The RH of $< 10\%$ in the DMA1 was obviously not low enough to dry the particles completely, and we presume that the measured particles were always present in a liquid state in the H-TDMA. Since liquid particles are spherical, no shape correction was applied (see ref 35).

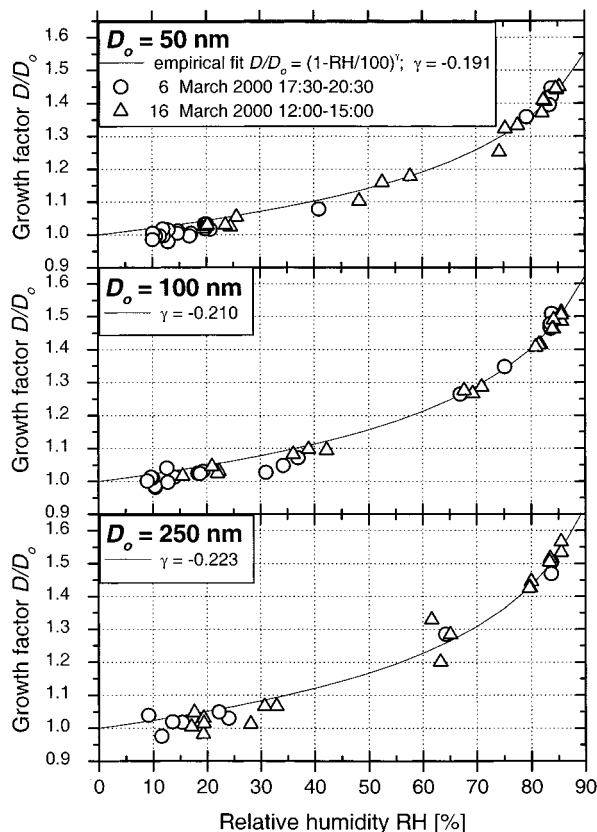


FIGURE 5. Humidograms of $D_o = 50, 100,$ and 250 nm particles measured at $T = -10\text{ }^\circ\text{C}$ during increasing RH scans at the high-alpine site Jungfraujoch located in the free troposphere. The greater scatter for the $D_o = 250\text{ nm}$ particles is due to very low number concentrations. The data points were acquired with a temporal resolution of 5 min.

The solid line in Figure 5 is an empirical model. The measured growth factors were fitted by the power law expression (21):

$$D/D_o = (1 - \text{RH}/100)^\gamma \quad (5)$$

where the RH is given in percent. The only unknown parameter γ was found to be $-0.191, -0.210,$ and -0.223 for $D_o = 50, 100,$ and 250 nm , respectively. This model fits the data well and can be used to extrapolate the hygroscopic growth to RH 90%, yielding $D/D_o = 1.55, 1.62,$ and 1.67 for $D_o = 50, 100,$ and 250 nm , respectively. In this campaign, the dry diameters D_o were determined by a comparison of the output of DMA1 with DMA2 at RH 10%. If one assumes that the particles still contain some water at this RH, then these growth factors are underestimated. This error can be estimated by means of the empirical model. According to eq 5, the particles exhibit a hygroscopic growth of $D/D_o \sim 1.02$ at RH 10%, which translates into an underestimation of measured growth factors by about 2%.

If one assumes that the particles are composed of an insoluble core with a hygroscopically inactive volume surrounded with soluble material, one can calculate the soluble volume fraction (ϵ). Such an analysis has the advantage that the size-dependent Kelvin effect is accounted for, allowing comparison of the hygroscopicity of particles at different sizes in terms of their chemical composition. The hygroscopically inactive volume can be water insoluble (such as elemental carbon), but it may also consist of water-soluble compounds that do not contribute significantly to the hygroscopic growth of particles [e.g., high molecular weight

organics such as humic acids as measured by Krivácsy et al. (47) at JFJ. Since $(\text{NH}_4)_2\text{SO}_4$ was found to be a major component (up to 40%) of the particulate mass at JFJ (47), $(\text{NH}_4)_2\text{SO}_4$ was chosen as the soluble component in this model. According to Pitchford and McMurry (48), for sufficiently soluble particles, ϵ is given by

$$\epsilon = (g_e^3 - 1)/(g_{\text{sol}}^3 - 1) \quad (6)$$

where g_e is the observed growth factor and g_{sol} is the theoretical growth factor of a fully soluble $(\text{NH}_4)_2\text{SO}_4$ particle at $T = -10^\circ\text{C}$ taken from ref 35. At RH 85%, ϵ is found to be 0.79, 0.86, and 0.91 for $D_o = 50, 100,$ and 250 nm, respectively. If the above-mentioned underestimation in the growth factor is taken into account, ϵ is increased to 0.86, 0.94, and 0.99 for $D_o = 50, 100,$ and 250 nm, respectively. It is interesting to note that ϵ increases with increasing particle size. We attribute this to different particle formation processes. Weingartner et al. (34) showed that especially during the colder seasons the smaller particles ($D < 20$ nm) at JFJ are predominately formed by (photo-) chemical reactions and may grow in size by gas-to-particle conversion whereas larger particles ($D > 100$ nm) are advected by (long-range) transport to the station. However, the detailed mechanisms leading to the observed hygroscopic behavior remain to be elucidated.

The determined growth factors at RH 90% can be compared with H-TDMA measurements performed at other remote sites. Swietlicki et al. (21) report H-TDMA measurements for $D < 50$ nm particles from Izaña, Tenerife (ES), at 2367 m above sea level. This station is influenced by the lower FT from time to time. At this site, bimodal growth spectra for $D_o = 50$ nm were measured ($D/D_o = 1.43$ and 1.62 for RH 90% and room temperature), which were attributed to a mixing of different air masses. It was supposed that the more hygroscopic particles probably originated from the marine boundary layer while the less hygroscopic mode was attributed to entrained particles from the lower FT. This is in contrast to our findings: In the FT at JFJ, particles were internally mixed with a higher growth factor (i.e. $D/D_o = 1.55$ at RH 90% for $D_o = 50$ nm and $T = -10^\circ\text{C}$). The reasons for these differences are at present unknown. One possible reason could be a different chemical FT air mass composition.

A future analysis of the JFJ H-TDMA data sets will provide further information to solve the question to what extent the chemical composition and thus the hygroscopicity of particles will change when they are heated from ambient to laboratory temperature.

Acknowledgments

The financial support of MeteoSwiss (Global Atmosphere Watch) is highly appreciated. In addition, we thank the International Foundation High Altitude Research Stations Jungfraujoch and Gornergrat (HFSJG), who made it possible for us to carry out our experiments at the High Altitude Research Station at Jungfraujoch. We also thank Silvia Henning, Nicolas Bukowiecki, Stefan Nyeki, András Hoffer, Matthias Weller, and Sebastian Schmidt for assistance in field work.

Literature Cited

- (1) Intergovernmental Panel on Climate Change (IPCC). *Climate Change 2001: The Scientific Basis*; Cambridge University Press: New York, 2001.
- (2) Kasten, F. *Tellus* **1969**, *21*, 631–635.
- (3) Hänel, G. *Adv. Geophys.* **1976**, *19*, 74–183.
- (4) Fitzgerald, J. W.; Hoppel, W. A.; Vietty, M. A. *J. Atmos. Sci.* **1982**, *39*, 1838–1852.
- (5) Twomey, S. *J. Atmos. Sci.* **1977**, *34*, 1149–1152.
- (6) Hitznerberger, R.; Berner, A.; Dusek, U.; Alabashi, R. *Aerosol Sci. Technol.* **1997**, *27*, 116–130.
- (7) Lee, C. T.; Hsu, W. C. *J. Aerosol Sci.* **2000**, *31*, 189–197.
- (8) Ohta, S.; Hori, M.; Yamagata, S.; Murao, N. *Atmos. Environ.* **1998**, *32*, 1021–1025.
- (9) Tang, I. N.; Munkelwitz, H. R. *Atmos. Environ.* **1993**, *27A*, 467–473.
- (10) Tang, I. N. *J. Geophys. Res.* **1997**, *102*, 1883–1893.
- (11) Tang, I. N.; Munkelwitz, H. R. *J. Appl. Meteorol.* **1994**, *33*, 791–796.
- (12) Rader, D. J.; McMurry, P. H. *J. Aerosol Sci.* **1986**, *17*, 771–787.
- (13) Liu, B. Y. H.; Pui, D. Y. H.; Whitby, K. T.; Kittelson, D. B.; Kousaka, Y.; McKenzie, R. L. *Atmos. Environ.* **1978**, *12*, 99–104.
- (14) Dougle, P. G.; Veeffkind, J. P.; tenBrink, H. M. *J. Aerosol Sci.* **1998**, *29*, 375–386.
- (15) Sekigawa, K. *J. Meteorol. Soc. Jpn.* **1983**, *61*, 359–366.
- (16) McMurry, P. H.; Stolzenburg, M. R. *Atmos. Environ.* **1989**, *23*, 497–507.
- (17) Covert, D. S.; Heinzenberg, J. *Atmos. Environ.* **1993**, *27*, 2989–2997.
- (18) Svenningsson, B.; Hansson, H. C.; Martinsson, B.; Wiedensohler, A.; Swietlicki, E.; Cederfelt, S. I.; Wendisch, M.; Bower, K. N.; Choulaton, T. W.; Colvile, R. N. *Atmos. Environ.* **1997**, *31*, 2463–2475.
- (19) Zhang, X. Q.; McMurry, P. H.; Hering, S. V.; Casuccio, G. S. *Atmos. Environ.* **1993**, *27*, 1593–1607.
- (20) Berg, O. H.; Swietlicki, E.; Krejci, R. *J. Geophys. Res.* **1998**, *103*, 16535–16545.
- (21) Swietlicki, E.; Zhou, J. C.; Covert, D. S.; Hameri, K.; Busch, B.; Vakeva, M.; Dusek, U.; Berg, O. H.; Wiedensohler, A.; Aalto, P.; Makela, J.; Martinsson, B. G.; Papaspiropoulos, G.; Mentes, B.; Frank, G.; Stratmann, F. *Tellus* **2000**, *52B*, 201–227.
- (22) Swietlicki, E.; Zhou, J. C.; Berg, O. H.; Martinsson, B. G.; Frank, G.; Cederfelt, S. I.; Dusek, U.; Berner, A.; Birmili, W.; Wiedensohler, A.; Yuskiewicz, B.; Bower, K. N. *Atmos. Res.* **1999**, *50*, 205–240.
- (23) Cocker, D. R.; Whitlock, N. E.; Flagan, R. C.; Seinfeld, J. H. *Aerosol Sci. Technol.* **2001**, *35*, 637–647.
- (24) Baltensperger, U.; Streit, N.; Weingartner, E.; Nyeki, S.; Prevot, A. S. H.; Van Dingenen, R.; Virkkula, A.; Putaud, J.-P.; Even, A.; ten Brink, H. M.; Blatter, A.; Neftel, A.; Gäggeler, H. W. *J. Geophys. Res.*, in press.
- (25) Cruz, C. N.; Pandis, S. N. *Environ. Sci. Technol.* **2000**, *34*, 4313–4319.
- (26) Saxena, P.; Hildemann, L. M.; McMurry, P. H.; Seinfeld, J. H. *J. Geophys. Res.* **1995**, *100*, 18755–18770.
- (27) Russell, A. G.; McRae, G. J.; Cass, G. R. *Atmos. Environ.* **1983**, *17*, 949–964.
- (28) Lugauer, M.; Baltensperger, U.; Furger, M.; Gäggeler, H. W.; Jost, D. T.; Schwikowski, M.; Wanner, H. *Tellus* **1998**, *50B*, 76–92.
- (29) Baltensperger, U.; Gäggeler, H. W.; Jost, D. T.; Lugauer, M.; Schwikowski, M.; Weingartner, E.; Seibert, P. *J. Geophys. Res.* **1997**, *102*, 19707–19715.
- (30) Nyeki, S.; Baltensperger, U.; Colbeck, I.; Jost, D. T.; Weingartner, E.; Gäggeler, H. W. *J. Geophys. Res.* **1998**, *103*, 6097–6107.
- (31) Nyeki, S.; Li, F.; Weingartner, E.; Streit, N.; Colbeck, I.; Gäggeler, H. W.; Baltensperger, U. *J. Geophys. Res.* **1998**, *103*, 31749–31761.
- (32) Lugauer, M.; Baltensperger, U.; Furger, M.; Gäggeler, H. W.; Jost, D. T.; Nyeki, S.; Schwikowski, M. *J. Geophys. Res.* **2000**, *105*, 19869–19879.
- (33) Zellweger, C.; Ammann, M.; Buchmann, B.; Hofer, P.; Lugauer, M.; Ruttimann, R.; Streit, N.; Weingartner, E.; Baltensperger, U. *J. Geophys. Res.* **2000**, *105*, 6655–6667.
- (34) Weingartner, E.; Nyeki, S.; Baltensperger, U. *J. Geophys. Res.* **1999**, *104*, 26809–26820.
- (35) Gysel, M.; Weingartner, E.; Baltensperger, U. *Environ. Sci. Technol.* **2002**, *36*, 63–68.
- (36) Wang, S. C.; Flagan, R. C. *Aerosol Sci. Technol.* **1990**, *13*, 230–240.
- (37) Endo, Y.; Fukushima, N.; Tashiro, S.; Kousaka, Y. *Aerosol Sci. Technol.* **1997**, *26*, 43–50.
- (38) Russell, L. M.; Flagan, R. C.; Seinfeld, J. H. *Aerosol Sci. Technol.* **1995**, *23*, 491–509.
- (39) Pruppacher, H. R.; Klett, J. D. *Microphysics of Clouds and Precipitation*, 2nd ed.; Kluwer Academic Publisher: Dordrecht, The Netherlands, 1997.
- (40) Oatis, S.; Imre, D.; McGraw, R.; Xu, J. *Geophys. Res. Lett.* **1998**, *25*, 4469–4472.

- (41) Hämeri, K.; Väkevä, M.; Hansson, H. C.; Laaksonen, A. *J. Geophys. Res.* **2000**, *105*, 22231–22242.
- (42) Neubauer, K. R.; Johnston, M. V.; Wexler, A. S. *Atmos. Environ.* **1998**, *32*, 2521–2529.
- (43) Braun, C.; Krieger, U. K. *Opt. Express* **2001**, *8*, 314–321.
- (44) Krieger, U. K.; Braun, C. *J. Quant. Spectrosc. Radiat. Transfer* **2001**, *70*, 545–554.
- (45) Busch, B.; Ferron, G.; Karg, E.; Silberg, A.; Heyder, J. *J. Aerosol Sci.* **1994**, *25*, S143–S144.
- (46) Weingartner, E.; Burtscher, H.; Baltensperger, U. *Atmos. Environ.* **1997**, *31*, 2311–2327.
- (47) Krivácsy, Z.; Gelencsér, A.; Kiss, G.; Mészáros, E.; Molnár, Á.; Hoffer, A.; Mészáros, T.; Sárvári, Z.; Temesi, D.; Varga, B.; Baltensperger, U.; Nyeki, S.; Weingartner, E. *J. Atmos. Chem.* **2001**, *39*, 235–259.
- (48) Pitchford, M. L.; McMurry, P. H. *Atmos. Environ.* **1994**, *28*, 827–839.

Received for review March 2, 2001. Revised manuscript received September 6, 2001. Accepted September 11, 2001.

ES010054O